Entanglement between a muon spin and $I > \frac{1}{2}$ nuclear spins

Pietro Bonfà,[1,*] Jonathan Frassineti,[2] John M. Wilkinson,[3] Giacomo Prando,[4] Muhammad Maikudi Isah,[1] Chennan Wang,[5] Tiziana Spina,[6] Boby Joseph,[7] Vesna F. Mitrović,[8] Roberto De Renzi,[9] Stephen J. Blundell,[3] and Samuele Sanna[2]

[1] *Department of Mathematical, Physical and Computer Sciences, University of Parma, Italy*
[2] *Department of Physics and Astronomy, University of Bologna, Italy*
[3] *Clarendon Laboratory, Department of Physics, University of Oxford, Parks Road, Oxford OX1 3PU, United Kingdom*
[4] *Department of Physics, University of Pavia, Italy*
[5] *Laboratory for Muon Spin Spectroscopy, Paul Scherrer Institute, CH-5232 Villigen, Switzerland*
[6] *Superconducting Radio Frequency (SRF) Materials and Research Department, Fermilab, Batavia, USA*
[7] *Elettra-Sincrotrone Trieste, S.S. 14-km 163.5, Basovizza, 34149 Trieste, Italy*
[8] *Department of Physics, Brown University, Providence, 02912 Rhode Island, USA*
[9] *Department of Mathematical, Physical and Computer Sciences, University of Parma, Italy*

(Dated: March 1, 2022)

We report on the first example of quantum coherence between the spins of muons and quadrupolar nuclei. We observe this effect in vanadium intermetallic compounds which adopt the A15 crystal structure, and whose members include all technologically dominant superconductors. The entangled states are extremely sensitive to the local structural and electronic environments through the electric field gradient at the quadrupolar nuclei. This case-study demonstrates that positive muons can be used as a quantum sensing tool to probe also structural and charge related phenomena in materials, even in the absence of magnetic order.

Quantum coherence between an implanted positively-charged muon and nuclei in a solid was first conclusively demonstrated using muon-spin spectroscopy (μSR) experiments on simple ionic fluorides [1]. The strong hydrogen-like bonding of the implanted positive muon (chemically identified as μ^+) to nearest-neighbor F ions, characterized by a single spin 1/2 ^{19}F nuclear isotope, gives rise to a hierarchical separation of the muon spin interactions. Typically, dipolar couplings with two nearest-neighbor (nn) ^{19}F nuclear spins, $\boldsymbol{I}_1$ and $\boldsymbol{I}_2$, determine the dominant spin-Hamiltonian of the $S = 1/2$ muon, whereas all the residual interactions, starting from the next nearest neighbors (nnn), can be ignored to a first approximation. Thanks to the 100% initial muon spin polarization, a prerogative of μSR, this shows up experimentally as a characteristic coherent spin precession pattern in the muon time-dependent asymmetry, uniquely determined by the geometry of the F–μ–F bonds. Many fluorinated compounds display this coherent pattern in non-magnetic phases, including ionic fluorides [2–4], fluropolymers [5, 6] and molecular magnets [7]. For these materials, the absence or the fast fluctuation of electronic magnetic moments leave the nuclear spin interactions to determine the dynamics of the muon spin polarization. This allows a very precise assignment of the muon implantation site, now known to be particularly accurate with the help of density functional theory (DFT) *ab-initio* simulations of the muon stopping-site inside the crystal (a technique which is also known as DFT+μ [8–12]). A similar coherent spin behavior has been identified in certain hydrides [13–15] and in metal–organic frameworks [16], where for instance a close association of a proton and the positive muon approximates a muoniated hydrogen molecule, μH, or possibly, a bonded molecular ion, $(\mu\mathrm{H})^+$, $(\mu\mathrm{H})^-$. Notice that ^{1}H, like ^{19}F, is a spin $I = 1/2$ nucleus.

In the case of H, as for the cases of many other nuclear species, such a coherent pattern is rarely observed in μSR experiments. Much more often a large number of unpolarized nuclear spins give rise to a T_2^{-1} relaxation process with either Gaussian or Lorentzian lineshapes, both the hallmarks of fast decoherence on the timescale of the period of the coherent quantum interference processes. Fluorine is special since it is very electronegative, and it has both a small ionic radius and a large nuclear moment, so that its dipolar coupling to the muon is strong and consequently several oscillations in any quantum-coherent signal can be observed before all muons have decayed or any nuclear relaxation process has become significant. The special F–μ–F case was very recently revisited by some of us [17], showing the role of the rest of the nuclear spins (nnn and beyond) in the slow decoherence process of F–μ–F. This work implies that the very well known F–μ–F effect, confined until now among the technicalities of the muon spectroscopy, displays all the features of a very high accuracy *quantum sensor* that can be exploited for microscopic detection of important physical phenomena [18]. Unfortunately, until now, the sensor has been available only for F$^-$- and, much more seldom, for H$^-$-containing materials.

In the present work we demonstrate the same surprising type of quantum coherence due to the entanglement of the muon spin with nn nuclear spin in the case of $I > 1/2$. We show this phenomenon in three intermetallic compounds, Nb_3Sn, V_3Si and V_3Sn, which belong to

* pietro.bonfa@unipr.it

This manuscript has been authored by Fermi Research Alliance, LLC under Contract No. DE-AC02-07CH11359 with the U.S. Department of Energy, Office of Science, Office of High Energy Physics.

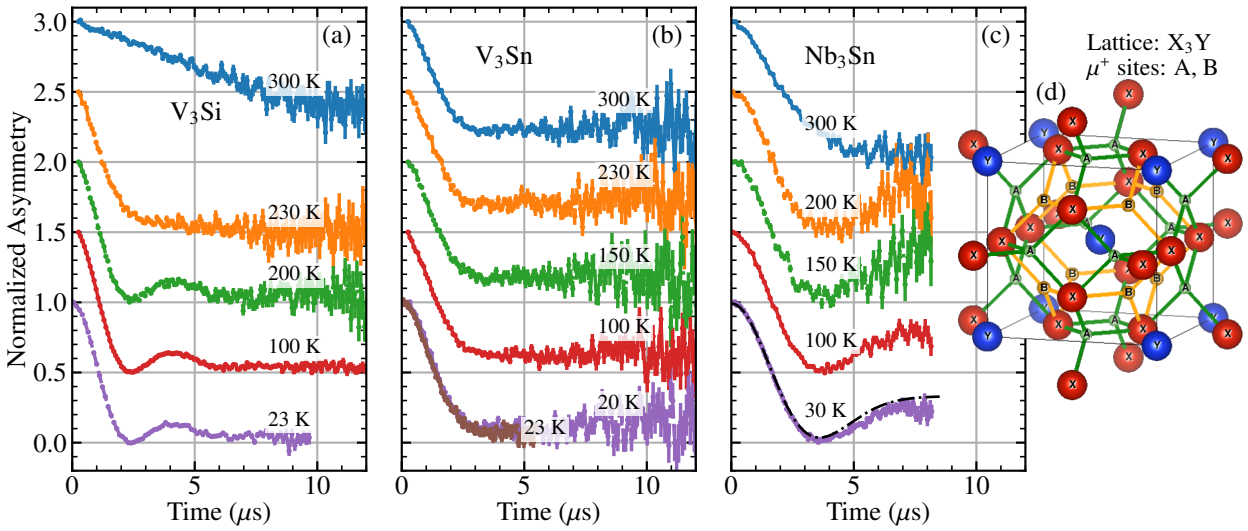

FIG. 1. Experimental results obtained for V_3Si (a), V_3Sn (b) and Nb_3Sn (c) at various temperatures in ZF. The initial asymmetry has been normalized to 1 and and the various measurements are shifted along the y axis by multiples of 0.5. The black line in (c) is a best fit to a static Kubo-Toyabe function. In picture (d) the lattice structure of A15 compounds and the candidate muon sites identified in this class of materials are depicted.

the A15 cubic phases ($Pm\bar{3}n$, group number 223), whose members include several technologically dominant conventional superconductors [19]. In stark contrast to the well-studied $I = 1/2$ case of ^{19}F and ^{1}H, the presence of nn nuclei with $I > 1/2$, namely $I = 7/2$, $9/2$ of ^{51}V and ^{93}Nb respectively, implies the existence of quadrupolar interactions. This has two effects that could potentially spoil the *quantum sensor* concept: first, it was until now unclear that a detectable quantum coherence could nevertheless show up in the muon asymmetry; second, quadrupolar interactions are proportional to the electric field gradient (EFG) at the nucleus in question, not just on the pure geometry of the bonds. EFG tensors are very accurately determined by DFT in bulk materials [20] and compared to the values measured for instance by nuclear magnetic resonance (NMR). The muon embedding in the crystal alters the bulk EFG in more than one way. We show that the coherent effect survives and we develop here an accurate model to describe this phenomenon. Our modeling of the coherence entails identifying precisely the muon site and calculating muon perturbed EFG tensors at nn and nnn nuclei. The results show that the observed phenomenon is highly sensitive to small structural and electronic differences among the same A15 family, paving the way to extend the use of muon spectroscopy as a quantum sensing technique for charge-related phenomena.

Zero-field (ZF) μSR temperature scans, using the EMU spectrometer at the ISIS Muon Source and the GPS spectrometer [21] at the Paul Scherrer Institute, have been conducted as a function of temperature. Further details on the experimental methods are provided in the Supplemental Material (SM)[22]. Fig. 1 shows the μSR spectra (time-dependent spin polarization of the muon ensemble) for all the samples at various representative temperatures. The temperature dependence is relatively weak, except above 200 K, where thermally activated μ^+ diffusion occurs [23]. At low temperature, where the muon is static in the μSR time window, the results are remarkably sample dependent despite all the X_3Y samples ($X = \{V, Nb\}$ and $Y = \{Si, Sn\}$) being very similar metals, sharing the same A15 cubic lattice structure. The structure is shown in Fig. 1d and our samples have a cubic lattice parameter a =4.72 Å, 4.98 Å, 5.29 Å for V_3Si, V_3Sn and Nb_3Sn respectively (see [22]), in agreement with previous results [24–26]. The nuclei of the X atoms are closer to the calculated muon sites, as shown in Fig. 1d with labels A and B, and all have similar properties: ^{51}V with 99.8% abundance has spin $I = 7/2$, gyromagnetic ratio $\gamma_V = 70.45\times10^6$ rad/(sT) and quadrupole moment Q =-0.052(10) barn and ^{93}Nb with 100% abundance has spin $I = 9/2$, $\gamma_{Nb} = 65.64 \times 10^6$ rad/(sT) and Q =-0.32(2) barn [27].

The oscillatory behavior observed in V_3Si (Fig. 1a) is in marked contrast to the cases of both Nb_3Sn (Fig. 1c), which resembles the conventional Kubo-Toyabe (KT) relaxation function (empirical KT best fit shown by the dashed line in the same panel and characterized by a dip and a tail that flattens at 1/3 of the initial value), and of V_3Sn (Fig. 1b), which could be described by a KT relaxation, with an additional decay of the 1/3 tail which has no evident physical origin. The surprisingly slow oscillations observed in V_3Si (Fig. 1a) cannot be due to internal fields of electronic origin since all these A15 samples are non-magnetic. Instead, as we will show, they result from a quantum coherent precession pattern due to the

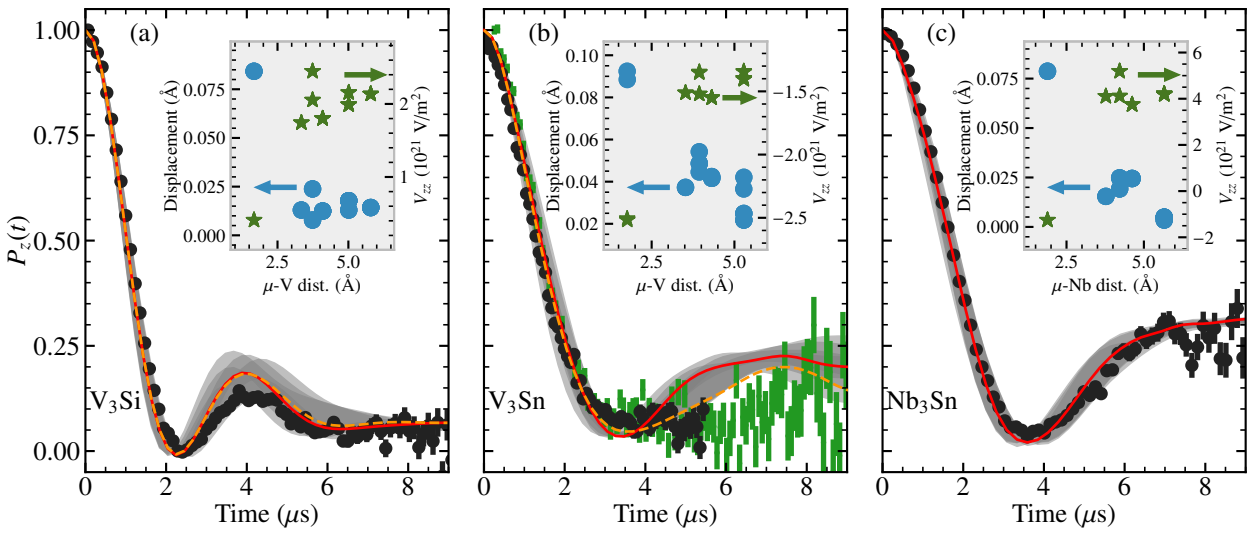

FIG. 2. Comparison between experimental and predicted muon spin polarization obtained using atomic displacements and EFGs from plane wave based DFT calculations. The black dots in panels a), b) and c) are lowest temperature data collected at PSI for V_3Si, V_3Sn and Nb_3Sn respectively. The green bars in panel (b) are ISIS results collected at 20 K. A background has been estimated by comparing the asymmetries collected at ISIS and PSI and removed. The red (orange) line in all plots is the depolarization obtained using first principles results from PW (FP) simulations to solve Eq. 1. Shaded area highlight different trends that originate by taking into account typical uncertainties of the DFT based predictions (see main text). The insets show the perturbation induced by the muon on its X-type neighbours (X =V,Nb). In particular, in the presence of the muon, the displacement of each X atom from its equilibrium position in the unperturbed lattice and the values of V_{zz} at the considered atomic site are reported on the left-hand and right-hand y-axes, respectively, as a function of the unperturbed distance of the considered atom from the μ^+ interstitial position in a 3x3x3 supercell.

coupling between the muon and nearby ^{51}V nuclear moments, analogous to the F–μ–F case, and never reported before for systems containing $I > 1/2$ nuclear spins.

In order to explain the three precession patterns of Fig. 1 we now consider the microscopic nuclear and electronic degrees of freedom entering the quantum mechanical model of the muon polarization. The model requires the knowledge of three ingredients to reproduce the experimental muon polarization: (i) the muon site, (ii) the perturbation induced by the μ^+ on the position of the neighboring atoms, (iii) the perturbation induced by the muon on the EFG at the nuclear sites with spin $I > 1/2$. These information allow to fully define the spin Hamiltonian $\mathcal{H}$ given by

$$\mathcal{H} = \sum_{i}^{N_{nuc}} \frac{\mu_0}{4\pi} \frac{\gamma_\mu \gamma_i \hbar^2}{r_i^3} \mathbf{S}_\mu \cdot \mathbf{D}^i \cdot \mathbf{I}^i + \frac{eQ_i}{2I(2I-1)} \mathbf{I}^i \cdot \mathbf{V}^i \cdot \mathbf{I}^i, \quad (1)$$

where $\mathbf{S}_\mu$ is the spin of the muon and r_i is its distance from nucleus i, $\mathbf{I}^i$ and Q_i are respectively the spin and the quadrupole moment of nucleus i, $\mathbf{D}$ and $\mathbf{V}$ are the dipolar and EFG tensors at nuclear site i, and other symbols have their standard meaning. All the quantities entering Eq. 1 can be accurately estimated with DFT-based *ab initio* approaches and we describe below the results that we obtained following the DFT+μ procedure.

Two candidate muon sites are present in our A15 compounds and are shown in Fig. 1d with labels A and B. Site A is located in the center of the tetrahedron formed by four X atoms while site B is in the center of the triangle formed by three X atoms. We find that site B always has higher energy than site A by hundreds of meV (see [22] for details) and is therefore omitted from the subsequent analysis. DFT simulations produce, as an additional outcome, the displacements of the atoms surrounding the muon. In all cases, the nn X atoms are substantially displaced by the muon and the nearest neighbor distances increase by 6%, 5%, 4% respectively in V_3Si, V_3Sn, Nb_3Sn (the absolute values are shown in the insets of Fig. 2 against the unperturbed μ-X distance and in SM [22]).

The next step is the evaluation of the EFG at the quadrupolar nuclei in each compound. While for ionic materials a point charge approximation may sometimes be sufficient, covalent and metallic systems require more elaborate strategies. Full potential (FP) DFT simulations yield very accurate estimates in materials where the mean field approximation does not break down owing to strong correlation, but are extremely computationally demanding. For this reason, and aiming at providing an easily adoptable approach, we opted for an effective compromise between accuracy and speed using a plane wave basis[28–30] combined with PAW [31] pseudopotentials. A detailed discussion of our strategy and additional comparisons with FP simulations[32] are provided in the SM [22]. Notably, this procedure converges much faster than

the equivalent technique aimed at the prediction of magnetic contact hyperfine fields at the muon sites [33].

Unsurprisingly, the EFG of the four X neighbors of the muon is drastically affected by the presence of the interstitial charge. For example, in V_3Si the unperturbed EFG tensor at V nuclei in the pristine material, with $V_{zz} = 2.2 \times 10^{21}$ V/m^2 and $\eta = 0$, in agreement with the experimental value of $V_{zz} = 2.37 \times 10^{21}$ V/m^2, reduces by almost an order of magnitude as a consequence of the presence of the positive impurity and the lattice distortion, in agreement with earlier work [23]. Note that site assignments come with some small uncertainty, and previous investigations that can be compared with experiment [17, 18, 34–36] reveal that a discrepancy of the order of a tenth of Angstrom is to be expected. On the other hand, plane wave based estimations of EFGs are subject to a much larger uncertainty of the order of 30% and 1.17×10^{21} V/m^2 in relative and absolute terms [37].

Having collected all parameters entering Eq. 1, we proceed to compute the time-dependent muon polarization numerically. For the A15 compounds the inter-nuclear dipolar interactions can be safely neglected[38] thus allowing the adoption of the approach proposed by Celio [39, 40] and implemented in the publicly available code UNDI [41], which makes the estimate very quick. Our calculations consider only effect of the nearest nuclei, but it has recently been shown by some of us [17] how to effectively include the effect of farther nuclei with an appropriate re-scaling of second nearest neighbors interaction, allowing a substantial reduction of the otherwise exponentially diverging dimension of the Hilbert space. Following [17], we consider 4 nn and 4 nnn whose positions are homogeneously rescaled by a small amount to compensate for the remaining nuclei (see [22] for details).

The predicted μSR signal obtained fully *ab initio*, i.e. without free parameters, is shown for all samples in Fig. 2 by a red line (PW results) and a orange dashed line (FP results), while shaded area indicate the uncertainty in the PW based prediction quantified with a reduction or increase of 3 % (29%) of $d_{\mu-X}$ (EFG values). Perfect agreement is found for Nb_3Sn [Fig. 2(c)], while for V_3Si [Fig. 2(a)] a small deviation is observed at about 4 μs where the first bump is slightly overestimated, although the experimental result falls inside the shaded area. A small increase of 15 mÅ in the μ-V distance allows to recover perfect agreement (see [22]). Remarkably the oscillation (the time position of minima and maxima) is very well reproduced. V_3Sn is the sample showing worst agreement in the long-time tail. In this case the deviation can be attributed to the limits of the PAW approximation in reconstructing the EFG at the V sites. Indeed the FP prediction, that differs from the PW based estimate by 16%, improves the agreement with the experimental data. These trends demonstrate the exquisite sensitivity of μSR to atomic distances and EFGs.

The striking difference between the muon asymmetries collected in a set of compounds that share the same lattice structure, the same muon site, and similar lattice distortions may appear puzzling at first sight. To address this point, we introduce the simple and analytically solvable case of one muon interacting with a single nucleus of spin I subject to an axial EFG [42]. In zero external field (ZF), the interaction depends on two parameters:

$$\omega_D = \frac{\mu_0}{4\pi}\frac{\gamma_\mu \gamma_I \hbar}{r_I^3}, \qquad \omega_Q = \frac{eV_{zz}Q}{4I\,(2I-1)\,\hbar}.$$

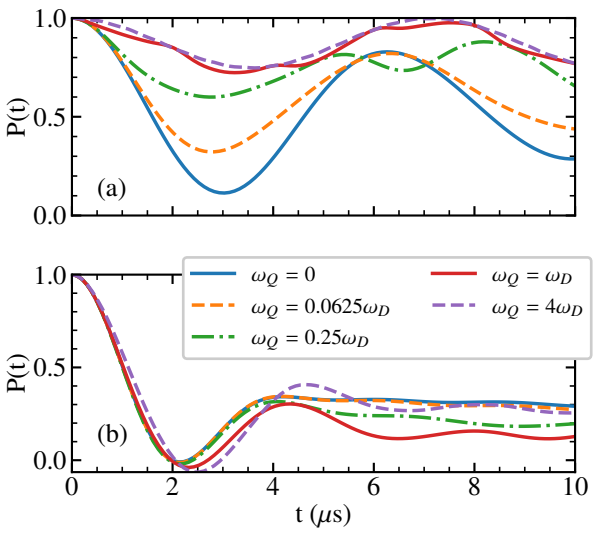

FIG. 3. (a) Time-dependent spin polarization $P(t)$ for a muon interacting with a single nucleus with spin $I = 7/2$ subject to an axial EFG for various values of ω_Q/ω_D. (b) $P(t)$ for a muon tetrahedrally coordinated to four $I = 7/2$ nuclei, all subject to the EFG generated by the muon itself.

Fig. 3a shows the muon polarization as a function of time for various values of ω_Q/ω_D for a single nuclear spin $I = 7/2$. This simple model illustrates how, in the two extreme regimes of zero and large quadrupolar splitting, the classical expectation of a single precession frequency is recovered, while, in intermediate regimes, multiple frequencies appear. Similarly, a departure from the semicalssical KT behaviour can also be appreciated in the more relevant case of a muon generating an EFG on four tetrahedrally coordinated $I = 7/2$ nuclei. The polarization as a function of time is obtained numerically in this case and shown in Fig. 3b. The trend recovers the 1/3 tail of the classical KT limit only in the small and large quadrupolar splitting conditions, while substantial deviations happen for the intermediate regime.

While the details of the muon polarizations in A15 compounds are connected to the peculiar composition of intrinsic and muon induced EFGs at the X sites, yielding to the simulated curves of Fig. 1, the behavior can be qualitatively understood considering the ratio $|\omega_Q|/\omega_D$ for the nn. Indeed this ratio happens to be about 2.4 for Nb_3Sn, 2 for V_3Sn, and 0.2 for V_3Si, thus qualitatively explaining the deviations from a KT-like trend of the latter two samples.

In conclusion, we have presented the experimental observation of coherent oscillations originating from the interaction between the muon and nuclei with $I = 7/2$. This signal is analogous to what has already been observed in fluorides and other materials containing $I = 1/2$ nuclei with high nuclear moments. An accurate description of the μSR spectra was obtained by solving parameter free spin Hamiltonians that consider the perturbed EFG at nuclear sites surrounding the muon and effectively include all nuclear spins in the system to correctly describe long-time depolarization. In μSR experiments the time evolution of the muon spin polarization depends dramatically upon the electronic distribution at quadrupolar nuclei coupled to the muon and an accurate estimation of the perturbed EFG at these sites is crucial for a successful analysis. We have shown that DFT based simulations can be effectively used to this aim and how their combination with simple spin Hamiltonians represents a computationally inexpensive method to accurately predict the μSR spectra of nuclear origin in virtually any crystalline material. The strong dependence of the μSR signal on the EFGs and the possibility of estimating quantitatively the perturbation of an interstitial μ^+ opens the possibility of using positive muons as a quantum sensing tool to probe also charge related phenomena in materials.

ACKNOWLEDGMENTS

The authors acknowledge Pascal Lejay for providing V_3Si and V_3Sn samples. This work is based on experiments performed at the Swiss Muon Source SμS, Paul Scherrer Institute, Villigen, Switzerland. We gratefully acknowledge the Science and Technology Facilities Council (STFC) for access to muon beamtime at the ISIS Neutron and Muon Source (EMU facility). S. S. thanks Consiglio Nazionale delle Ricerche (CNR) for supporting his visit at ISIS. We thank René Flükiger for support for sample selection, Franz Lang and Peter Baker for support during the experiment at ISIS. V. F. M. acknowledges support of the National Science Foundation grant #DMR-1905532. P. B., M. M. I and R. D. R. acknowledge funding from the SUPER (Supercomputing Unified Platform - Emilia-Romagna) regional project and computing power form STFC's SCARF cluster.

[1] J. H. Brewer, S. R. Kreitzman, D. R. Noakes, E. J. Ansaldo, D. R. Harshman, and R. Keitel, Observation of muon-fluorine "hydrogen bonding" in ionic crystals, Phys. Rev. B **33**, 7813(R) (1986).

[2] D. R. Noakes, E. J. Ansaldo, S. R. Kreitzman, and G. M. Luke, The $(F\mu F)^-$ ion in solid fluorides, J. Phys. Chem. Solids **54**, 785 (1993).

[3] T. Lancaster, S. J. Blundell, P. J. Baker, W. Hayes, S. R. Giblin, S. E. McLain, F. L. Pratt, Z. Salman, E. A. Jacobs, J. F. C. Turner, and T. Barnes, Intrinsic magnetic order in Cs_2AgF_4 detected by muon-spin relaxation, Phys. Rev. B **75**, R220408 (2007).

[4] T. Lancaster, F. L. Pratt, S. J. Blundell, I. McKenzie, and H. E. Assender, Muon–fluorine entanglement in fluoropolymers, J. Phys.: Condens. Matter **21**, 346004 (2009).

[5] F. L. Pratt, S. J. Blundell, I. M. Marshall, T. Lancaster, A. Husmann, C. Steer, W. Hayes, C. Fischmeister, R. E. Martin, and A. B. Holmes, μSR in polymers, Physica B **326B**, 34 (2003).

[6] K. Nishiyama, S. W. Nishiyama, and W. Higemoto, Asymmetric F–μ–F interaction of the muon in polyfluorocarbons, Physica B **326B**, 41 (2003).

[7] T. Lancaster, S. J. Blundell, P. J. Baker, M. L. Brooks, W. Hayes, F. L. Pratt, J. L. Manson, M. M. Conner, and J. A. Schlueter, Muon-fluorine entangled states in molecular magnets, Phys. Rev. Lett. **99**, 267601 (2007).

[8] F. Bernardini, P. Bonfà, S. Massidda, and R. De Renzi, Ab initio strategy for muon site assignment in wide band gap fluorides, Phys. Rev. B **87**, 115148 (2013).

[9] J. S. Möller, D. Ceresoli, T. Lancaster, N. Marzari, and S. J. Blundell, Quantum states of muons in fluorides, Phys. Rev. B **87**, 121108 (2013).

[10] J. S. Möller, P. Bonfà, D. Ceresoli, F. Bernardini, S. J. Blundell, T. Lancaster, R. D. Renzi, N. Marzari, I. Watanabe, S. Sulaiman, and M. I. Mohamed-Ibrahim, Playing quantum hide-and-seek with the muon: localizing muon stopping sites, Physica Scripta **88**, 068510 (2013).

[11] P. Bonfá and R. De Renzi, Toward the computational prediction of muon sites and interaction parameters, Journal of the Physical Society of Japan **85**, 091014 (2016).

[12] S. J. Blundell, R. D. Renzi, T. Lancaster, and F. L. Pratt, Chapter 16, in *Muon spectroscopy – an introduction* (Oxford University Press, 2022).

[13] J. Lord, S. Cottrell, and W. Williams, Muon spin relaxation in strongly coupled systems, Physica B: Condensed Matter **289-290**, 495 (2000).

[14] P. Mendels, F. Bert, M. A. de Vries, A. Olariu, A. Harrison, F. Duc, J. C. Trombe, J. S. Lord, A. Amato, and C. Baines, Quantum magnetism in the paratacamite family: Towards an ideal kagomé lattice, Phys. Rev. Lett. **98**, 077204 (2007).

[15] R. Kadono, K. Shimomura, K. H. Satoh, S. Takeshita, A. Koda, K. Nishiyama, E. Akiba, R. M. Ayabe, M. Kuba, and C. M. Jensen, Hydrogen bonding in sodium alanate: A muon spin rotation study, Phys. Rev. Lett. **100**, 026401 (2008).

[16] G. Prando, J. Perego, M. Negroni, M. Riccò, S. Bracco, A. Comotti, P. Sozzani, and P. Carretta, Molecular rotors in a metal–organic framework: Muons on a hyper-fast carousel, Nano Letters **20**, 7613 (2020).

[17] J. M. Wilkinson and S. J. Blundell, Information and decoherence in a muon-fluorine coupled system, Phys. Rev. Lett. **125**, 087201 (2020).

[18] J. M. Wilkinson, F. L. Pratt, T. Lancaster, P. J. Baker, and S. J. Blundell, Muon sites in PbF_2 and YF_3: Decohering environments and the role of anion Frenkel defects, Phys. Rev. B **104**, L220409 (2021).

[19] J. Muller, A15-type superconductors, Rep. Prog. Phys. **43**, 641 (1980).

[20] P. Blaha, K. Schwarz, and P. Herzig, First-principles calculation of the electric field gradient of Li_3N, Phys. Rev. Lett. **54**, 1192 (1985).

[21] A. Amato, H. Luetkens, K. Sedlak, A. Stoykov, R. Scheuermann, M. Elender, A. Raselli, and D. Graf, The new versatile general purpose surface-muon instrument (GPS) based on silicon photomultipliers for μSR measurements on a continuous-wave beam, Review of Scientific Instruments **88**, 093301 (2017).

[22] See Supplemental Material at [URL will be inserted by publisher] for additional details concerning the experimental setting and the results of DFT simulations. Input and output data to reproduce our results are available via Materials Cloud [43].

[23] A. Yaouanc, O. Hartmann, E. Karlsson, E. Wäckelgård, R. Wäppling, D. Druchart, R. Fruchart, and J. P. Senateur, Transverse field μ^+SR study of V_3Si, Hyper. Inter. **31**, 93 (1986).

[24] C. Paduani and C. A. Kuhnen, Martensitic phase transition from cubic to tetragonal V_3Si: an electronic structure study, Eur. Phys. J. B **66**, 353 (2008).

[25] N. Morton, B. James, G. Wostenholm, and N. Howard, The resistivity of V_3Sn and related compounds, Journal of the Less Common Metals **64**, 69 (1979).

[26] A. Alimenti, N. Pompeo, K. Torokhtii, T. Spina, R. Flükiger, L. Muzzi, and E. Silva, Microwave measurements of the high magnetic field vortex motion pinning parameters in Nb_3Sn, Superconductor Science and Technology **34**, 014003 (2020).

[27] Multiple inconsistent results have been published for the quadrupole moments of ^{51}V and ^{94}Nb. We used recommended values from IAEA available at https://www-nds.iaea.org/nuclearmoments/isotope_measurement_results.php?A=51&Z=23 and https://www-nds.iaea.org/nuclearmoments/isotope_measurement_results.php?A=93&Z=41.

[28] P. Giannozzi, O. Baseggio, P. Bonfà, D. Brunato, R. Car, I. Carnimeo, C. Cavazzoni, S. de Gironcoli, P. Delugas, F. Ferrari Ruffino, A. Ferretti, N. Marzari, I. Timrov, A. Urru, and S. Baroni, Quantum ESPRESSO toward the exascale, The Journal of Chemical Physics **152**, 154105 (2020).

[29] P. Giannozzi, S. Baroni, N. Bonini, M. Calandra, R. Car, C. Cavazzoni, D. Ceresoli, G. L. Chiarotti, M. Cococcioni, I. Dabo, A. Dal Corso, S. de Gironcoli, S. Fabris, G. Fratesi, R. Gebauer, U. Gerstmann, C. Gougoussis, A. Kokalj, M. Lazzeri, L. Martin-Samos, N. Marzari, F. Mauri, R. Mazzarello, S. Paolini, A. Pasquarello, L. Paulatto, C. Sbraccia, S. Scandolo, G. Sclauzero, A. P. Seitsonen, A. Smogunov, P. Umari, and R. M. Wentzcovitch, QUANTUM ESPRESSO: a modular and open-source software project for quantum simulations of materials, Journal of Physics: Condensed Matter **21**, 395502 (19pp) (2009).

[30] P. Giannozzi, O. Andreussi, T. Brumme, O. Bunau, M. B. Nardelli, M. Calandra, R. Car, C. Cavazzoni, D. Ceresoli, M. Cococcioni, N. Colonna, I. Carnimeo, A. D. Corso, S. de Gironcoli, P. Delugas, R. A. D. Jr, A. Ferretti, A. Floris, G. Fratesi, G. Fugallo, R. Gebauer, U. Gerstmann, F. Giustino, T. Gorni, J. Jia, M. Kawamura, H.-Y. Ko, A. Kokalj, E. Küçükbenli, M. Lazzeri, M. Marsili, N. Marzari, F. Mauri, N. L. Nguyen, H.-V. Nguyen, A. O. de-la Roza, L. Paulatto, S. Poncé, D. Rocca, R. Sabatini, B. Santra, M. Schlipf, A. P. Seitsonen, A. Smogunov, I. Timrov, T. Thonhauser, P. Umari, N. Vast, X. Wu, and S. Baroni, Advanced capabilities for materials modelling with QUANTUM ESPRESSO, Journal of Physics: Condensed Matter **29**, 465901 (2017).

[31] P. E. Blöchl, Projector augmented-wave method, Phys. Rev. B **50**, 17953 (1994).

[32] The Elk Code, http://elk.sourceforge.net/.

[33] I. J. Onuorah, P. Bonfà, and R. De Renzi, Muon contact hyperfine field in metals: A DFT calculation, Phys. Rev. B **97**, 174414 (2018).

[34] A. Amato, P. Dalmas de Réotier, D. Andreica, A. Yaouanc, A. Suter, G. Lapertot, I. M. Pop, E. Morenzoni, P. Bonfà, F. Bernardini, and R. De Renzi, Understanding the μsr spectra of mnsi without magnetic polarons, Phys. Rev. B **89**, 184425 (2014).

[35] N. Martin, M. Deutsch, F. Bert, D. Andreica, A. Amato, P. Bonfà, R. De Renzi, U. K. Rößler, P. Bonville, L. N. Fomicheva, A. V. Tsvyashchenko, and I. Mirebeau, Magnetic ground state and spin fluctuations in MnGe chiral magnet as studied by muon spin rotation, Phys. Rev. B **93**, 174405 (2016).

[36] J. S. Möller, D. Ceresoli, T. Lancaster, N. Marzari, and S. J. Blundell, Quantum states of muons in fluorides, Phys. Rev. B **87**, 121108 (2013).

[37] K. Choudhary, J. N. Ansari, I. I. Mazin, and K. L. Sauer, Density functional theory-based electric field gradient database, Scientific Data **7**, 10.1038/s41597-020-00707-8 (2020).

[38] The X-X atom distance is of the order of 3 Å, about 1.75 times larger than $d_{\mu-X}$. We have also verified that internuclear interactions marginally affect the depolarization signal.

[39] M. Celio, A new technique to calculate the muon polarization function, Hyperf. Inter. **31**, 41 (1986).

[40] M. Celio, New method to calculate the muon polarization function, Phys. Rev. Lett. **56**, 2720 (1986).

[41] P. Bonfà, J. Frassineti, M. M. Isah, I. J. Onuorah, and S. Sanna, Undi: An open-source library to simulate muon-nuclear interactions in solids, Comp. Phys. Comm. **260**, 107719 (2021).

[42] S. Vogel, M. Celio, and P. F. Meier, Calculation of the muon polarization function for longitudinal fields, Hyperfine Interactions **31**, 35 (1986).

[43] P. Bonfà, J. Frassineti, J. M. Wilkinson, G. Prando, M. M. Isah, C. Wang, T. Spina, B. Joseph, V. F. Mitrović, R. D. Renzi, S. J. Blundell, and S. Sanna, Entanglement between a muon spin and $I > 1/2$ nuclear spins, https://dx.foi.org/10.24435/materialscloud:7j-vg (2022).